Experimental and theoretical study of the hyperfine structure in the lower configurations in ^{45}Sc II

P. Villemoes,* R. van Leeuwen,† A. Arnesen, F. Heijkenskjöld, A. Kastberg, and M. O. Larsson
Department of Physics, Uppsala University, Box 530, S-751 21 Uppsala, Sweden

S. A. Kotochigova
State Optical Institute, 199 034 St. Petersburg, Russia
(Received 15 November 1991)

We have measured the hyperfine structure (hfs) of 12 levels in the configurations $3d4s$, $3d^2$, and $3d4p$ in singly ionized scandium by collinear fast-ion-beam–laser spectroscopy. The hfs of the four levels in the configuration $3d4s$ has to our knowledge not been measured before. From these levels the ions were excited to levels in the $3d4p$ configuration by the frequency-doubled output of a ring dye laser with an intracavity mounted $LiIO_3$ crystal. Levels in the $3d^2$ configuration were excited to levels in the $3d4p$ configuration with visible laser light. The resulting magnetic dipole (A) and electric quadrupole (B) hfs constants are analyzed in Sandars-Beck effective-operator formalism. The multiconfiguration Dirac-Fock method has been used to calculate the hfs constants for levels in the configurations $3d4s$, $3d5s$, $3d6s$, $3d^2$, and $3d4p$. Within the framework of the configuration-interaction method, an approach is presented for the calculation of the core polarization, which uses a virtual basis set localized inside the core. For all levels, this approach gives better results compared to previously published calculations.

PACS number(s): 35.10.Fk, 31.30.Gs, 32.30.Jc

I. INTRODUCTION

High-resolution measurements of hyperfine structure (hfs) provide a test of *ab initio* calculations, and thus a step towards a satisfactory description of the interaction between the nucleus and the electrons. Knowledge about the hfs is also useful for a correct interpretation of spectra from stars. A broad hyperfine splitting can have a large effect on the elemental abundance deduced from lines with low excitation energy in stellar analysis [1]. Several investigations of the hfs in $3d$ elements (e.g., Refs. [2] and [3] and references therein) show that the contact contribution to the hfs induced by the $3d$ shell on the core shells, i.e., the core polarization, is large. To find a means of predicting the hfs for levels of, e.g., astrophysical interest we must first understand the effect of core polarization. In this paper we present an experimental and theoretical investigation of the magnetic dipole (A) and electric quadrupole (B) hyperfine coupling constants for levels in the lowest configurations in singly ionized scandium.

We have measured the hfs of 12 levels in the configurations $3d4s$, $3d^2$, and $3d4p$ in Sc II. The hfs of levels in the two latter configurations has been investigated previously. The first article was published by Arnesen *et al.* in 1982 [4], and since then accurate measurements have been reported by Young *et al.* [5] and Mansour *et al.* [6]. The knowledge of the hfs of the $3d^2$ and the $3d4p$ configurations is almost complete due to the ultrahigh resolution obtained with the laser-rf double-resonance technique used by Mansour *et al.* [6]; but until now no measurements have been performed in the lowest configuration $3d4s$. The reason for this is that the levels in the closest odd configuration $3d4p$ are not accessible by single photon excitation with visible laser light. We have used frequency-doubled laser light to avoid this problem. Figure 1 shows a partial energy-level scheme of the lower levels in Sc II where the transitions we have studied are indicated. The experimentally determined magnetic-dipole (A) and electric-quadrupole (B) coupling constants are analyzed in the framework of the effective-operator formalism [7] in order to extract information about the most important contributions to the hfs.

The singly charged scandium ion is a fairly simple system, having two valence electrons, which makes it a suitable object for theoretical studies. The only stable isotope is ^{45}Sc with nuclear spin $I=\frac{7}{2}$. The nuclear magnetic-dipole moment is $\mu_I=4.7559\,\mu_N$ (μ_N is the nuclear magneton) and the electric quadrupole moment is $Q=-0.22$ b [8]. Mansour *et al.* [6] used the multiconfiguration Dirac-Fock (MCDF) method for *ab initio* calculations of the hfs coupling constants. They showed that the MCDF approach gives good results for the singlet states, but that the core-polarization effect must be included in order to compute accurate A values for the triplet states. We have obtained theoretical values for the A and B constants for a number of configurations ($3d4s$, $3d5s$, $3d6s$, $3d^2$, $3d4p$, and $4s4p$), using the MCDF method in an attempt to understand the disagreements between experiment and theory in Ref. [6]. Particular emphasis has been given to the calculations of the hfs constants for the two lowest even configurations, since they are most sensitive to a polarization of the core shells.

The configuration-interaction (CI) approach is often used to describe the spin density at the nucleus caused by the core polarization [9–15]. This kind of calculation employs a large set of single-particle basis functions, where configuration interaction between various levels is

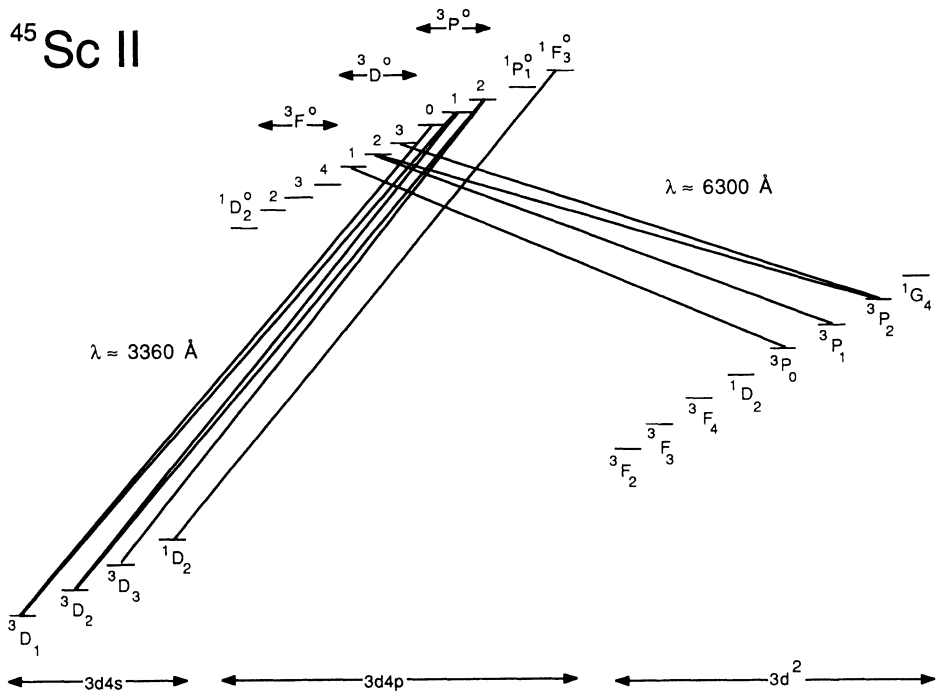

FIG. 1. Partial energy level scheme of the lower configurations in singly ionized scandium. The transitions we have studied are indicated.

accounted for. Slater-type orbitals (STO's) are often preferred for the description of basis functions [11,16], but in some cases a Gaussian basis is employed for computational reasons [17–20]. One of the aims of the present study is to suggest an alternative approach for the description of core polarization. The emphasis will be on the construction of a basis from sophisticated atomic wave functions [such as Dirac-Fock (DF) functions], including a set of virtual states with one-electron excitation of the core shells, without excessive demands for computer storage. The CI wave functions are given in terms of a full set of modified DF functions which are located inside the core.

In the first part of the paper we describe the experimental setup (Sec. II A) followed by the experimental results for the A and B constants (Sec. II B) and an interpretation of the constants in the effective-operator formalism (Sec. II C). In Sec. III we introduce our approach for the MCDF calculations. The first step is to calculate the hfs coupling constants assuming a frozen core (Sec. III B), and in Sec. III C this approach is extended to the application of core polarization.

II. EXPERIMENT

A. Experimental setup

The main features of the experimental setup at the Uppsala isotope separator are shown in Fig. 2. The ions are produced in an arc-discharge ion source, extracted through a circular aperture, and accelerated to a kinetic energy of about 30 keV. After acceleration, the ions are mass analyzed through a double-focusing magnet. The ion current is monitored by deflecting the ion beam into a Faraday cup after the laser-interaction region. The scandium ions are excited by light from a stabilized cw ring dye laser (CR-699) pumped by an argon ion laser. The frequency scans are calibrated by directing a portion of the visible output of the dye laser through a confocal Fabry-Pérot interferometer (FPI), with a free spectral range of 298.6(5) MHz, corresponding to 597 MHz in the

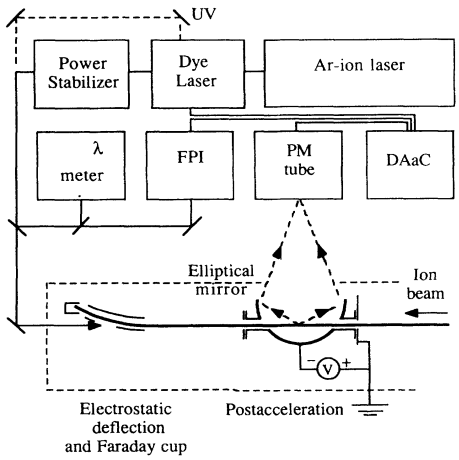

FIG. 2. Main features of the experimental setup for hfs measurements at the Uppsala isotope separator. (FPI = Fabry-Pérot interferometer, PM = photomultiplier, and DAaC = data acquisition and control).

UV, and the wavelength is measured with a scanning Michelson interferometer. Table I gives a list of the studied transitions.

The visible laser light used for the excitation of the $3d^2$ configuration was stabilized with a commercial laser-power stabilizer to keep the laser background constant. Filters are used to suppress detection of scattered laser light. For the excitation of the levels in the $3d4s$ configuration we have used an angle-tuned, intracavity-mounted, frequency-doubling crystal ($LiIO_3$). The power of the UV radiation is of the order of 1 mW.

The laser-induced fluorescence (LIF) is directed into a photomultiplier tube by an elliptical mirror with a light-collecting efficiency of near 50% including solid angle and reflectance. The metallic elliptical mirror has a conducting wire grid in front of it; the mirror and the grid constitute a Faraday cage, which defines the laser–ion-beam interaction region. When the ions reach this region they experience the postacceleration potential of the Faraday cage and are Doppler shifted into resonance with the counterpropagating laser beam. Typical LIF spectra for Sc II recorded with UV light are shown in Fig. 3. The observed linewidth full width at half maximum (FWHM) is about 60 MHz for the lines excited with visible laser light and 120 MHz for UV excitation. The width results from natural lifetime broadening and Doppler broadening. The transit time broadening is negligible since the ions are in resonance much longer than the natural lifetimes.

The first hfs measurements in Sc II, reported by Arnesen *et al.* [4], were performed using an acceleration voltage of 230 kV. The spectral linewidths achieved in that experiment were typically 150 MHz. This is more than a factor of 2 larger than in the present experiment. As stated in Ref. [4] the gain in resolution due to more efficient velocity bunching with the 230-kV accelerator is concealed partly by a larger energy spread in the ion source and partly by a larger ripple in the acceleration voltage than in our low-energy accelerator. Also, a misalignment between the laser and ion beam will contribute more severely to the linewidth at higher acceleration voltage. In the present experiment the common beam path of the laser and ion beams is defined by circular apertures of 2-mm diameter at the entrances to the Faraday cage confining the interaction region. The alignment can be optimized by maximizing the throughput of the transmitted laser light and ion-beam current.

TABLE I. A list of the studied transitions in Sc II.

Levels		Laser λ	Number of
Lower	Upper	in air (Å)	spectra
$3d4s\ ^1D_2$	$3d4p\ ^1F_3^\circ$	3353.73	8
$3d4s\ ^3D_2$	$3d4p\ ^3P_2^\circ$	3359.68	8
$3d4s\ ^3D_1$	$3d4p\ ^3P_1^\circ$	3361.27	8
$3d4s\ ^3D_1$	$3d4p\ ^3P_0^\circ$	3361.94	8
$3d4s\ ^3D_2$	$3d4p\ ^3P_1^\circ$	3368.95	8
$3d4s\ ^3D_3$	$3d4p\ ^3P_2^\circ$	3372.15	6
$3d^2\ ^3P_2$	$3d4p\ ^3D_3^\circ$	6245.63	8
$3d^2\ ^3P_1$	$3d4p\ ^3D_2^\circ$	6279.76	8
$3d^2\ ^3P_2$	$3d4p\ ^3D_2^\circ$	6300.70	8
$3d^2\ ^3P_0$	$3d4p\ ^3D_1^\circ$	6309.90	8

B. Experimental results

The frequency scale is obtained by fitting the positions of the reference peaks from the FPI to a Legendre polynomial. The positions of the spectral lines are then determined by fitting the line profile to a Gaussian function. From these data, the hyperfine coupling constants A and B are derived using the well-known expression

$$E_{\rm hfs}=\tfrac{1}{2}AC+\tfrac{1}{2}B\frac{3C(C+1)-4I(I+1)J(J+1)}{2I(2I-1)2J(2J-1)}\ , \qquad (1)$$

where $C=F(F+1)-I(I+1)-J(J+1)$ and J, I, and F are the quantum numbers of the electronic angular momentum, the nuclear spin, and the total atomic angular momentum, respectively. Contributions from higher-order terms cannot be resolved in our experiment. The experimentally determined A and B constants are given in Table II, columns 3 and 6. The first column in Table II lists the energy of the levels in the studied configurations. In the second column we give the percentage of the LS-coupled leading term. This is discussed further in Sec. II C. The best results obtained with the *ab initio* calculations described in Sec. III are given in columns 4 and 7, followed by the difference between experiment and theory. Since there are misprints in Ref. [6], Table III, we list our results together with previous measurements. The uncertainties presented within parentheses are two standard deviations of the mean, corresponding to an almost 95% confidence interval. They result mainly from random fluctuations of experimental parameters such as the acceleration voltage and the energy spread in the ion source. The Doppler shift correction ($\Delta\nu_0 v/c$) is accounted for in the A and B constants. For scandium ions, accelerated with 30 kV, the Doppler-shift correction will be 1.2 MHz/1000 MHz (0.12%). There are some disagreements between present and previous measurements, but they are not systematic. All results for the B constants agree within error bars but only three agree for the A values.

The spectrum of the transition $3d4s\ ^3D_1\rightarrow 3d4p\ ^3P_0^\circ$ has only three components, so the two constants have to be derived from two equations, which is an unfavorable situation. The result for the $3d4s\ ^3D_1$ level is $A=-478.9(8)$ MHz and $B=-14(2)$ MHz. (Uncertainties are given in parentheses.) The values derived from the transition $3d4s\ ^3D_1\rightarrow 3d4p\ ^3P_1^\circ$ are $A=-483(2)$ MHz and $B=-4(8)$ MHz. The weighted means of these results are presented in Table II, but we must point out the fact that there are large uncertainties, both in value and in sign, of the B constant for this level.

C. Interpretation of results in the effective-operator formalism

An extensive investigation of the spectrum of singly ionized scandium in the region 1100–11 000 Å was made

by Johansson and Litzén [21]. There is a high degree of overlap between the two systems $3dnl$ and $4snl$ in Sc II, which may cause configuration interaction of the levels we are studying. However, for the high even configurations it was found that the interaction between the $3dnd$ and $3d(n+1)s$, $n=4,5$, was weak. In order to see if this holds also for the low even configurations $3d4s$ and $3d^2$, we have made a least-squares fit of

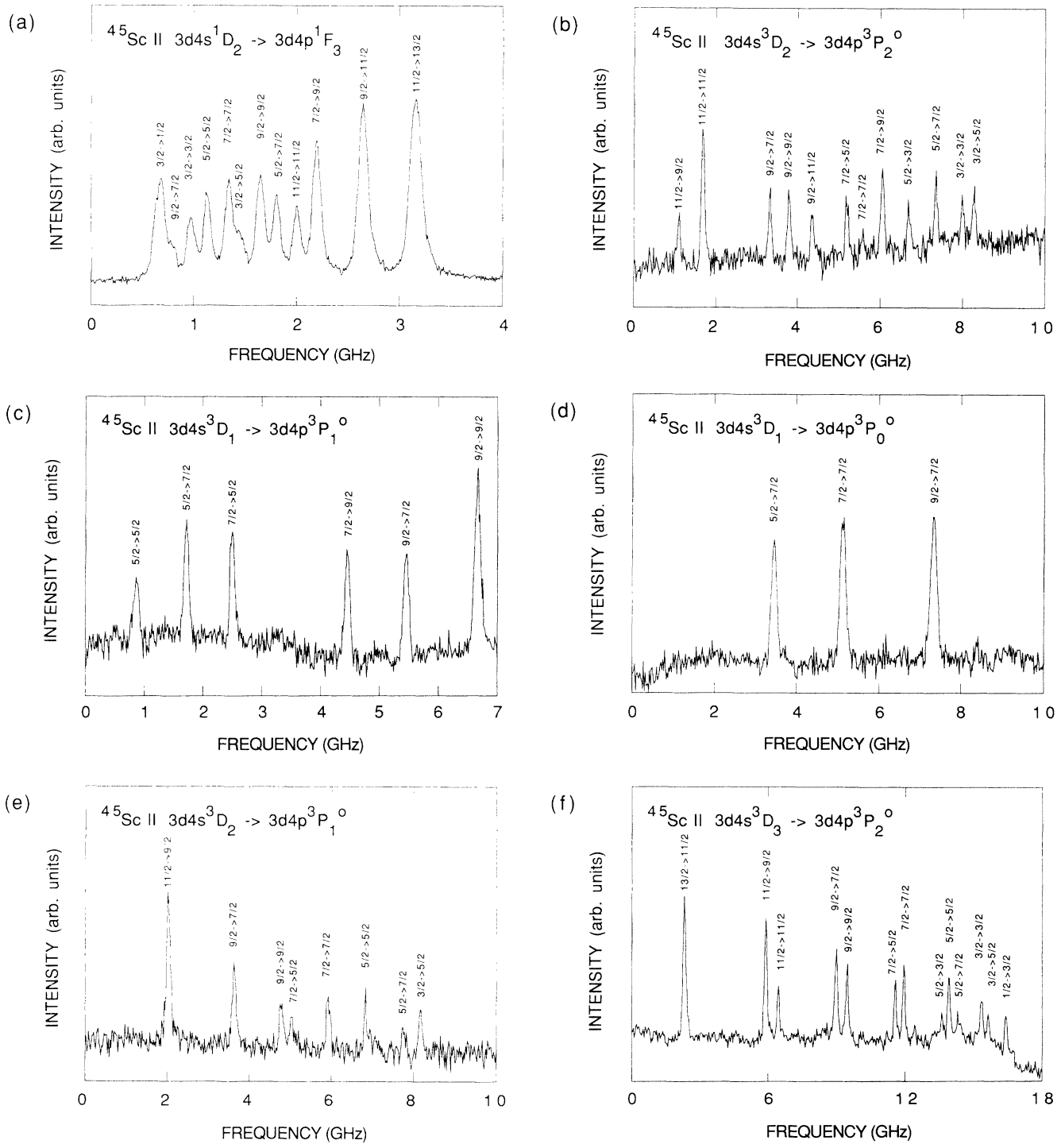

FIG. 3. Recorded hfs spectra for the transitions from the ground configuration $3d4s$ to the lowest odd configuration $3d4p$ in Sc II. The transitions are induced by frequency-doubled laser light. (a) The transition $3d4s\ ^1D_2 \rightarrow 3d4p\ ^1F_3^\circ$. (b) The transition $3d4s\ ^3D_2 \rightarrow 3d4p\ ^3P_2^\circ$. (c) The transition $3d4s\ ^3D_1 \rightarrow 3d4p\ ^3P_1^\circ$. (d) The transition $3d4s\ ^3D_1 \rightarrow 3d4p\ ^3P_0^\circ$. (e) The transition $3d4s\ ^3D_2 \rightarrow 3d4p\ ^3P_1^\circ$. (f) The transition $3d4s\ ^3D_3 \rightarrow 3d4p\ ^3P_2^\circ$.

intermediate-coupling theoretical level energies in terms of Slater integrals and fine-structure coupling constants to experimental level energies [22], as described by, e.g., Condon and Shortley [23]. The level $3d^2\,{}^1S_0$ was excluded in the fit. The corresponding eigenvectors are, neglecting terms smaller than 0.1%,

$$
\begin{aligned}
&|3d4s\,{}^3D_1'\rangle = |3d4s\,{}^3D_1\rangle\ ,\\
&|3d4s\,{}^3D_2'\rangle = 0.999|3d4s\,{}^3D_2\rangle + 0.035|3d4s\,{}^1D_2\rangle\ ,\\
&|3d4s\,{}^3D_3'\rangle = |3d4s\,{}^3D_3\rangle\ ,\\
&|3d4s\,{}^1D_2'\rangle = 0.996|3d4s\,{}^1D_2\rangle + 0.076|3d^2\,{}^1D_2\rangle\\
&\qquad\qquad - 0.035|3d4s\,{}^3D_2\rangle\ ;
\end{aligned}
\tag{2}
$$

$$
\begin{aligned}
&|3d^2\,{}^3F_2'\rangle = |3d^2\,{}^3F_2\rangle\ ,\\
&|3d^2\,{}^3F_3'\rangle = |3d^2\,{}^3F_3\rangle\ ,\\
&|3d^2\,{}^3F_4'\rangle = |3d^2\,{}^3F_4\rangle\ ,\\
&|3d^2\,{}^1D_2'\rangle = 0.995|3d^2\,{}^1D_2\rangle - 0.076|3d4s\,{}^1D_2\rangle\\
&\qquad\qquad - 0.062|3d^2\,{}^3P_2\rangle\ ,\\
&|3d^2\,{}^3P_1'\rangle = |3d^2\,{}^3P_1\rangle\ ,\\
&|3d^2\,{}^3P_2'\rangle = -0.998|3d^2\,{}^3P_2\rangle - 0.063|3d^2\,{}^1D_2\rangle\ ,\\
&|3d^2\,{}^1G_4'\rangle = |3d^2\,{}^1G_4\rangle\ ,
\end{aligned}
\tag{3}
$$

where $\zeta_{3d}(3d4s) = 71\ \text{cm}^{-1}$, and $\zeta_{3d}(3d^2) = 48\ \text{cm}^{-1}$ with a χ of 17 cm^{-1} ($\chi = [\sum_n \Delta^2/(n-m)]^{1/2}$; n is the number

TABLE II. A list of experimental and calculated hyperfine coupling constants for the configurations $3d4s$, $3d4p$, and $3d^2$ in Sc II. The uncertainties presented within parentheses for the experimental values are two standard deviations of the mean. The calculated values are the best obtained with the methods described in Sec. III.

Level	Energy (cm^{-1})	Leading LS term (%)	A_{meas} (MHz)	A_{calc} (MHz)	ΔA (MHz)	B_{meas} (MHz)	B_{calc} (MHz)	ΔB (MHz)
$3d4s\,{}^3D_1$	0.0	100	−480(2)[a]	−473.3	7	−13(3)[a]	11.8	25
$3d4s\,{}^3D_2$	67.72	100	510(1)[a]	518.8	9	−30(12)[a]	−13.0	17
$3d4s\,{}^3D_3$	177.76	100	654.8(6)[a]	608.5	−46	−63(23)[a]	−35.5	28
$3d4s\,{}^1D_2$	2 540.95	99	128.2(8)[a]	146.8	19	−39(11)[a]	−25.5	14
$3d^2\,{}^3F_2$	4 802.87	100	290.67(4)[b]	277.6	−13	−10.5(2)[b]	−8.9	2
$3d^2\,{}^3F_3$	4 883.57	100	113.672(6)[b]	137.5	24	−12.62(8)[b]	−28.9	16
$3d^2\,{}^3F_4$	4 987.79	100	38.357(4)[b]	60.9	23	−16.5(2)[b]	−38.1	22
$3d^2\,{}^1D_2$	10 944.56	99	149.361(4)[b]	146.0	−3	7.818(6)[b]	10.4	3
$3d^2\,{}^3P_1$	12 101.50	100	−108.1(4)[a]	−63.6	44	−13(2)[a]	−16.9	−4
			−107.501(4)[b]			−12.30(2)[b]		
$3d^2\,{}^3P_2$	12 154.42	100	−27.2(4)[a]	−0.03	27	26(3)[a]	18.2	−8
			−27.732(4)[b]			22.127(6)[b]		
$3d^2\,{}^1G_4$	14 261.32	100	135.232(2)[b]	154.6	19	−63.44(8)[b]	−99.1	−36
$3d4p\,{}^1D_2^\circ$	26 081.34	99	215.7(8)[c]	202.5	−13	18(7)[c]	−10.8	−29
$3d4p\,{}^3F_2^\circ$	27 443.71	99	366.8(3)[d]	425.3	58	−40(28)[d]	−31.7	8
$3d4p\,{}^3F_3^\circ$	27 602.45	99	205.4(12)[d]	193.7	−12	−70(36)[d]	−58.5	12
$3d4p\,{}^3F_4^\circ$	27 841.35	100	102.3(2)[b]	115.6	14	−84(4)[b]	−76.0	8
$3d4p\,{}^3D_1^\circ$	27 917.78	100	307(2)[a]	267.7	−39	1(8)[a]	−0.7	−2
			304.7(4)[b]			4(2)[b]		
$3d4p\,{}^3D_2^\circ$	28 021.29	99	125.7(3)[a]	149.0	23	6(3)[a]	−11.7	−18
			125.3(2)[b]			10(2)[b]		
$3d4p\,{}^3D_3^\circ$	28 161.17	99	101.8(6)[a]	128.3	27	24(9)[a]	−13.1	−37
			99.5(2)[b]			21(4)[b]		
$3d4p\,{}^3P_1^\circ$	29 742.16	92	258(2)[a]	148.0	−110	12(6)[a]	11.4	−1
			255.0(4)[b]			10(16)[b]		
$3d4p\,{}^3P_2^\circ$	29 823.93	94	105.6(5)[a]	87.2	−18	−21(4)[a]	−13.6	7
			106.2(2)[b]			−20(2)[b]		
$3d4p\,{}^1F_3^\circ$	32 349.98	100	193.1(8)[a]	184.9	−8	−65(14)[a]	−86.3	−21
			191.1(6)[b]			−82(8)[b]		

[a]New measurements.
[b]Reference [6].
[c]Reference [4].
[d]Reference [5].

of levels included in the fit ($n=12$) and m the number of parameters ($m=8$)[24]). The levels have high purity in the LS coupling scheme. Furthermore, Mansour *et al.* [6] estimated the off-diagonal hfs interactions for the levels in the $3d^2$ configuration and found that only perturbations from members of the same fine-structure multiplet were significant. In the most severe case ($3d^2\,{}^3P_1$) this was reported to influence the A value less than 70 kHz, and the B value less than 1 MHz.

Johansson and Litzén [21] concluded that also the levels of the $3d4p$ configuration have clear LS character (Table II). Even though there is a high degree of overlap between the configurations $3dnl$ and $4snl$, they found that the only significant interactions are those between $4s4p$ and $3d4p$ in the ${}^1P_1$ and the ${}^3P_{0,1,2}$ levels. Fitted values of the fine-structure constants for the odd configurations ($3d4p+3d5p+4s4p$) were reported to be $\zeta_{3d}=79\ \mathrm{cm}^{-1}$ and $\zeta_{4p}=179\ \mathrm{cm}^{-1}$.

We have analyzed the results in the framework of the semiempirical effective-operator method [7]. The A and B hyperfine coupling constants are expressed as linear combinations of the effective radial parameters $a_{nl}^{k_s k_l}$ and $b_{nl}^{k_s k_l}$, using the matrix elements given by Childs [25]. The effective radial parameters are defined as

$$a_{nl}^{k_s k_l}=\frac{\mu_0}{4\pi}2\mu_B\frac{\mu_I}{I}\langle r^{-3}\rangle_{nl}^{k_s k_l}\ , \tag{4}$$

$$b_{nl}^{k_s k_l}=\frac{e^2}{4\pi\epsilon_0}Q\langle r^{-3}\rangle_{nl}^{k_s k_l}\ , \tag{5}$$

where a_{nl}^{10} is the contact parameter. For light elements, where relativistic effects are likely to be negligible, this contribution to the hfs from the nl ($l\neq 0$) electron comes from interaction with the core shells $1s^2$, $2s^2$, and $3s^2$ (core polarization) or via configuration interaction with a neighboring configuration containing an s electron. The contact parameter may be large for $3d$ elements. The effective Hamiltonian taking into account configuration interaction between levels with the same L, S, and J has the same form as the effective Hamiltonian for relativistic effects [7], and therefore the configuration interaction in (2) and (3) is included in the radial parameters derived from experiment. We assume that other configuration-interaction effects are negligible. Then in the nonrelativistic limit $a_{nl}=a_{nl}^{01}=a_{nl}^{12}$, $b_{nl}=b_{nl}^{02}$, and $b_{nl}^{11}=b_{nl}^{13}=0$. As a test of the importance of relativistic effects, we have performed a least-squares fit of the accurate data for the $3d^2$ levels in Ref. [6], given in Table II, to the linear combinations of radial parameters in both the relativistic and the nonrelativistic limit. The result in the pure LS case is summarized in Table III (V_{rms} is the root-mean-square value ($V_{\mathrm{rms}}=[\sum_n \Delta^2/n]^{1/2}$)[24]). The fact that we have nonzero values for b_{3d}^{13} and b_{3d}^{11}, and that a_{3d}^{12} is smaller than a_{3d}^{01}, can be explained by the unstable situation of the coupled equations caused by the small contributions of these parameters. We therefore conclude that relativistic effects are small and derive other parameters in the nonrelativistic limit. The result for the $3d^2$ configuration is then, from Table III,

$$\begin{aligned} &a_{3d}=143.3\ \mathrm{MHz},\quad a_{3d}^{10}=-229.6\ \mathrm{MHz}\ ,\\ &b_{3d}=-55.0\ \mathrm{MHz}\ . \end{aligned} \tag{6}$$

The contact contribution to the $3d$ shell is large and negative in sign with respect to the a_{3d} parameter.

For the $3d4s$ configuration we have a system of four equations with two unknowns, a_{3d} and C, where $C=a_{4s}^{10}+a_{3d}^{10}$. A least-squares fit in the pure LS case yields

$$\begin{aligned} &a_{3d}=180.4(5)\ \mathrm{MHz},\quad C=3388(4)\ \mathrm{MHz}\ ,\\ &V_{\mathrm{rms}}=36\ \mathrm{MHz}\ ; \end{aligned} \tag{7}$$

$$b_{3d}=-90(19)\ \mathrm{MHz},\quad V_{\mathrm{rms}}=9.1\ \mathrm{MHz}\ . \tag{8}$$

The errors presented originate from the uncertainties (two standard deviations of the mean) in the A and B constants derived from experiment. If we only consider the levels that are purely LS coupled, we get a solution that is exact for the dipole parameters

$$a_{3d}=175.8(7)\ \mathrm{MHz},\quad C=3325(3)\ \mathrm{MHz}\ . \tag{9}$$

For the $3d4p$ configurations we have ten levels, eight of which have a 99–100% LS coupled leading term, and three unknowns: a_{3d}, a_{4p}, and C', where $C'=a_{3d}^{10}+a_{4p}^{10}$. The system is solved by using the weighted averages of the measured hyperfine coupling constants given in Table II. The result is, assuming pure LS coupling,

$$\begin{aligned} &a_{3d}=223.8(2)\ \mathrm{MHz},\quad a_{4p}=139.3(5)\ \mathrm{MHz}\ ,\\ &C'=-13.7(7)\ \mathrm{MHz}\ ,\quad V_{\mathrm{rms}}=31\ \mathrm{MHz}\ ; \end{aligned} \tag{10}$$

$$\begin{aligned} &b_{3d}=-72(9)\ \mathrm{MHz},\quad b_{4p}=-98(9)\ \mathrm{MHz}\ ,\\ &V_{\mathrm{rms}}=6.0\ \mathrm{MHz}\ . \end{aligned} \tag{11}$$

Using only the eight levels with high purity in LS coupling yields

$$\begin{aligned} &a_{3d}=189.3(2)\ \mathrm{MHz},\quad a_{4p}=216.0(5)\ \mathrm{MHz}\ ,\\ &C'=-182.6(7)\ \mathrm{MHz}\ ,\quad V_{\mathrm{rms}}=9.7\ \mathrm{MHz}; \end{aligned} \tag{12}$$

TABLE III. Effective radial parameters for the $3d^2$ configuration derived from experimental A and B constants in Ref. [6] given in Table II.

(MHz)	a_{3d}^{01}	a_{3d}^{12}	a_{3d}^{10}	V_{rms}	b_{3d}^{02}	b_{3d}^{13}	b_{3d}^{11}	V_{rms}
Relativistic	144.0	128.8	−235.1	5.6	−54.8	6.0	−5.7	2.2
Nonrelativistic	143.3	143.3	−229.6	6.1	−55.0	0.0	0.0	2.3

TABLE IV. Effective radial parameters derived from experimental A and B constants in Table II. (a) The magnetic dipole interaction. $C=a_{3d}^{10}+a_{4s}^{10}$ and $C'=a_{3d}^{10}+a_{4p}^{10}$. (b) The electric quadrupole interaction.

(a)

(MHz)	a_{3d}	a_{4p}	a_{3d}^{10}	C	C'
$3d4s$	175.8(7)			3325(3)	
$3d^2$	143.3		−229.6		
$3d4p$	189.3(2)	216.0(5)			−182.6

(b)

(MHz)	b_{3d}	b_{4p}
$3d4s$	−90(19)	
$3d^2$	−55	
$3d4p$	−71(9)	−98(9)

$$b_{3d}=-71(9)\ \text{MHz},\quad b_{4p}=-98(9)\ \text{MHz}\ ,\qquad V_{\text{rms}}=6.6\ \text{MHz}\ . \tag{13}$$

Omitting the two levels $3d4p\ ^3P_{1,2}$, which have a mixing of 6% of $4s4p\ ^3P_{1,2}$, has a large effect on the magnetic-dipole parameters, and naturally a most dramatic effect on the induced contact parameter. It has no significant effect on the electric-quadrupole parameters. We summarize the result for the effective radial parameters from (6,8,9,12,13) in Table IV. The a_{3d} and b_{3d} parameters are clearly not configuration independent. The value of the radial integrals in the effective radial parameters a_{nl} [Eq. (4)] and b_{nl} [Eq. (5)] can be expressed in terms of the spin-orbit coupling constant ζ_{nl} as

$$\langle r^{-3}\rangle_{nl}=\xi_{nl}[a_0^3 hcR_y\alpha^2 Z_i H(l,Z_i)]^{-1}\ , \tag{14}$$

where $H(l,Z_i)$ is a relativistic correction factor [26]. Table V lists the obtained values for the effective radial parameters from the spin-orbit coupling constants $\zeta_{3d}=79\ \text{cm}^{-1}$ and $\zeta_{4p}=179\ \text{cm}^{-1}$ given by Johansson and Litzén [21] for the odd configurations ($3d4p+3d5p+4s4p$) and the values $\zeta_{3d}(3d^2)=48\ \text{cm}^{-1}$ and $\zeta_{3d}(3d4s)=71\ \text{cm}^{-1}$ obtained in the calculation of the eigenvectors (2) and (3) for the even configurations ($3d4s+3d^2$). The ratio $a_{3d}(3d4s)/a_{3d}(3d4p)$ is 0.93 from experiment and 0.90 from the spin-orbit coupling constants. Corresponding values for $a_{3d}(3d^2)/a_{3d}(3d4p)$ are 0.76 and 0.61. The rather good agreement between the values of the effective radial parameters obtained from experiment and from spin-orbit constants (Tables IV and V) indicates that the hfs could be estimated in the effective-operator approach if the contact parameter could be derived.

TABLE V. Effective radial parameters derived from the spin-orbit coupling constants $\zeta_{3d}(3d4s)=71\ \text{cm}^{-1}$, $\zeta_{3d}(3d^2)=48\ \text{cm}^{-1}$, $\zeta_{3d}(3d4p)=79\ \text{cm}^{-1}$, and $\zeta_{4p}=179\ \text{cm}^{-1}$.

(MHz)	a_{3d}	a_{4p}	b_{3d}	b_{4p}
$3d4s$	157		−63	
$3d^2$	106		−42	
$3d4p$	175	232	−70	−93

III. THEORY

A. The MCDF formalism for calculation of hfs constants

The atomic hyperfine structure is caused by several interactions. The strongest of these is the magnetic-dipole interaction involved in the coupling of the nuclear spin I, the electron orbital angular momentum **L**, and spin **S** if $I\neq 0$. The next strongest is the interaction between the nuclear quadrupole moment **Q**, and the electric field gradient produced at the nucleus by the surrounding electrons.

The magnetic interaction can be separated into two parts: the dipole or anisotropic interaction and the isotropic interaction. The magnetic-dipole coupling constant A contains contributions from both these parts. The isotropic interaction A_{iso} is produced by the spin of unpaired electrons inside the core, whereas the dipole contribution A_{aniso} can be obtained assuming that all core shells have zero total angular momentum and no unpaired electrons. This means that the spin density at the nucleus produced by the core electrons in filled shells is zero. We will calculate A_{aniso} using the MCDF method, assuming that the core wave functions are frozen and taking into account mixing between closely lying configurations [27]. There are various ways to choose a frozen-core potential, keeping in mind the different kinds of configurations of valence electrons in the self-consistent field process. Section III B contains concrete details of this procedure.

Unfortunately, the above-mentioned method often fails in reproducing experimental results. In this case a significant contribution to the A constant originates, as expected, from the isotropic part. It has been recognized for two-electron systems [6] that this term should be important mainly in triplet atomic states. A solution to this problem is to use different wave functions for electrons in the closed shells that differ only in their spin directions, i.e., we introduce a polarization of the core shells. We have used the CI formalism to describe the core polarization. The virtual basis set has been represented through functions offering similar properties to Sturm's functions. They are localized inside the core and include the continuum. The specific property of our approach is the small size of the basis set (Sec. III C). It is well known that the full set of Hamiltonian eigenvalues of the atomic system contains both discrete and continuous components. This means that the total set of eigenfunctions includes the continuous functions as well. As a result, not only summation over the discrete levels, but also integration over the continuum, should be made in the calculation of matrix elements with mixing of configurations. This is difficult to realize. In order to overcome this problem we use a full set of discrete functions in our approach. The development of a full set of eigenvalue functions for the discrete spectrum was first suggested by Schrödinger in 1926 [28]. This kind of function has been used by Hylleraas [29] for two-electron atomic calculations. The role

of the continuum in the superposition of configurations was investigated by Shull and Löwdin [30]. It was shown that the absence of continuous functions in the full basis set leads to a significant improvement of the convergence compared with the hydrogen functions. An early application to hfs calculations was made by Lunell [31], using a spin-polarized frozen-core approximation.

B. MCDF frozen-core approximation

The total wave function of the atomic state contains both an electron part $\Phi(J,m_J)$ and a nuclear part $\Theta(I,m_I)$, and can be written as

$$\Psi(F,m_F)=\sum_{m_I,m_J}\langle F,m_F|I,J;m_I,m_J\rangle\Phi(J,m_J)\Theta(I,m_I)\ , \tag{15}$$

where m_J,m_I, and m_F are the magnetic quantum numbers, and $\langle F,m_F|I,J;m_I,m_J\rangle$ the Clebsh-Gordan coefficients. In first-order perturbation theory the energy contribution from the magnetic-dipole interaction to the hyperfine structure levels is

$$\Delta E_\mu(F,m_F)=\langle F,m_F|W_\mu|F,m_F\rangle\ , \tag{16}$$

where

$$W_\mu=\sum_i r_i^{-3}g_I\mu_N(I[\mathbf{r}_i\times\boldsymbol{\alpha}_i])\ , \tag{17}$$

and g_I is the gyromagnetic ratio, $\mu_N=eh/(4\pi mc)$, and α is the Dirac matrix. Inserting (17) into (16) we obtain after some transformations

$$\Delta E_\mu(F,m_F)=\sum_{m_I,m_J}\sum_{m_I',m_J'}\langle F,m_F|I,J;m_I,m_J\rangle\langle F,m_F|I,J;m_I',m_J'\rangle \times g_I\mu_N\sum_\nu(-1)^\nu\langle I,m_I|I_\nu|I,m_I'\rangle\left\langle J,m_J\left|\sum_i r_i^{-3}(\mathbf{r}_i\times\boldsymbol{\alpha}_i)_\nu\right|J,m_J'\right\rangle\ , \tag{18}$$

where $\nu=m_J-m_J'$. Using the relation

$$\langle I,m_I|I_\nu|I,m_I'\rangle=\langle I,m_I|I,1;m_I',\nu\rangle[I(I+1)]^{1/2}\ , \tag{19}$$

we transform the matrix elements of (18) in the frame of irreducible-tensor operators using the Wigner-Eckart theorem. This leads to the following expression:

$$\Delta E_\mu(F,m_F)=g_I\mu_N[J(J+1)(2J+1)]^{-1/2} \times[F(F+1)-J(J+1)-I(I+1)] \times\left\langle J\left|\left|\sum_i r^{-3}[\mathbf{r}_i\times\boldsymbol{\alpha}_i]_0\right|\right|J\right\rangle\ , \tag{20}$$

where the reduced matrix element is independent of the quantum numbers m, so we may choose $m_J=m_J'$, i.e., $\nu=0$. However, taking into account that the DF wave functions are linear combinations of Slater determinants, which are eigenfunctions of the operator $\mathbf{J}_z$, we may calculate the total wave function for a fixed value of $m_J=m_C$. Here we have applied the so-called M representation. After diagonalization of the energy matrix it is possible to obtain a set of states that are eigenfunctions of the operator $\mathbf{J}$. These states have different values of J, but the same m_J. A second application of the Wigner-Eckart theorem gives, with $\mathbf{V}=\sum_i r^{-3}[\mathbf{r}_i\times\boldsymbol{\alpha}_i]_0$:

$$\langle J\|\mathbf{V}\|J\rangle=\frac{(-1)^k\langle J,m_C|\mathbf{V}|J,m_C\rangle(2J+1)^{1/2}}{\langle J,m_C|J,1;m_C,0\rangle}\ , \tag{21}$$

and the relation $\langle J,m_C|J,1;m_C,0\rangle=m_C[J(J+1)]^{-1/2}$ $(J\neq0)$ leads to the hyperfine energy

$$\Delta E_\mu(F,m_F)=A[F(F+1)-J(J+1)-I(I+1)]/2\ . \tag{22}$$

Here,

$$A(J)=g_I\mu_N\left\langle J,m_C\left|\sum_i r^{-3}[\mathbf{r}_i\times\boldsymbol{\alpha}_i]_0\right|J,m_C\right\rangle\Big/m_C \tag{23}$$

is the magnetic-dipole coupling constant, which depends only on the electronic states.

Consider now the matrix element of (23) in the many-configuration approximation, where $|J,m_C\rangle=\sum_\alpha c_\alpha\det_\alpha$ is expressed through the Dirac spinors $|a\rangle$

$$|a\rangle=\begin{bmatrix}P_a(r)/r & \Omega_{k_a m_a}\\ -iQ_a(r)/r & \Omega_{-k_a m_a}\end{bmatrix}\ , \tag{24}$$

where P_a is the large and Q_a the small component of the radial wave function, Ω_{km} its spin-orbital part, and c_α are coefficients of mixing of configurations. After evaluation, the one-electron matrix element takes the form

$$\langle a|r^{-3}[\mathbf{r}\times\boldsymbol{\alpha}]_0|b\rangle=[(2j_b+1)/(2j_a+1)]^{1/2} \times(k_a+k_b)\langle j_a,m_a|j_b,1;m_b,0\rangle \times\langle j_a,\tfrac{1}{2}|1,j_b;0,\tfrac{1}{2}\rangle \times\int dr\,r^{-2}(P_aQ_b+Q_aP_b)\ , \tag{25}$$

where k_a and k_b are the relativistic quantum numbers of the states a and b.

The total matrix element is

$$\left\langle J,m_C \left| \sum_i r_i^{-3}[\mathbf{r}_i \times \boldsymbol{\alpha}_i]_0 \right| J,m_C \right\rangle = \sum_{\alpha,\beta} c_\alpha c_\beta \left\langle \det_\alpha \left| \sum_i r_i^{-3}[\mathbf{r}_i \times \alpha_i]_0 \right| \det_\beta \right\rangle . \quad (26)$$

The expressions for the quadrupole interaction can be obtained in a similar way. The one-electron matrix element is given by

$$\langle a|r^{-3}\mathbf{Y}_{20}|b\rangle = [(2j_b+1)/(2j_a+1)]^{1/2} \times \langle j_a,m_a|j_b,2;m_b,0\rangle \langle j_a,\tfrac{1}{2}|2,j_b;0,\tfrac{1}{2}\rangle \times \int dr\, r^{-3}(P_aP_b+Q_aQ_b) . \quad (27)$$

Here we have used the M representation of the matrix elements in the same way as above. The total matrix element has the form

$$\left\langle J,m_C \left| \sum_i r^{-3}\mathbf{Y}_{20} \right| J,m_C \right\rangle = \sum_{\alpha,\beta} c_\alpha c_\beta \left\langle \det_\alpha \left| \sum_i r^{-3}Y_{20} \right| \det_\beta \right\rangle . \quad (28)$$

The shift of an energy level due to the quadrupole interaction is given by the relation

$$\Delta E_Q(F,m_F) = \frac{B[3F(F+1)-4I(I+1)J(J+1)]}{2[2I(2I-1)2J(2J-1)]} , \quad (29)$$

where

$$B = 2Q[2J(2J-1)(2J+1)/(2J+2)(2J+3)]^{1/2} \times \langle J,m_C|r^{-3}Y_{20}|J,m_C\rangle/m_C \quad (30)$$

is the electric-quadrupole coupling constant in atomic units and Q is the nuclear quadrupole moment.

C. Core-polarization approach

Numerous attempts have been made to calculate the core-polarization effect in atoms. Most of these calculations have employed the CI method, using a large basis set. For example, CI treatments based on a Gaussian basis set need a few thousand configurations to recover more than 90% of the correlation energy [15]. The CI method with mixing of various levels of sophistication is very similar in spirit to our approach, but there are major distinctions.

One is that the conventional method uses DF solutions as a virtual basis set, while we construct special functions, which have similarities to Sturm's basis, in order to describe the correlation problem. The full set of DF solutions contains the wave functions of both discrete levels and the continuum. This means that the continuum should be included in the basis set in order to obtain accurate values of hfs constants, which, however, leads to serious computational problems. This is why it is preferable to include the continuum in the functions.

Another distinction is that DF solutions generate orbitals with average radii, which grow very rapidly with increasing excitation energy. In other words, the traditional method uses a basis set, which has to be very large in order to obtain accurate values of the hfs constants. In this work, the radial parts of the virtual orbitals have the form

$$\phi_c(r) = f_c(r)r^n , \quad (31)$$

where $n=1,2,\ldots,$ and $f_c(r)$ is the radial DF function of a core orbital. The orbitals (31) are then orthogonalized with respect to the low-lying orbitals. These virtual orbitals have the same average radii as the f_c functions, and a large basis set is, therefore, not needed to describe the correlation interaction efficiently. Moreover, they include both discrete and continuous spectrum components. Basis sets similar to ours have been used before in the frame of the HF method, e.g., in Refs. [30–33].

We have calculated the polarization effect for the ground and several excited states of Sc II. The partly occupied valence shells cause an uncompensated spin density at the nucleus via the fully occupied core shells. As a result, the magnetic hfs constant A of the valence levels must be corrected by the addition of $A_{\rm iso}$. We do not aim to calculate the total value of $A_{\rm iso}$, summing the spin-density correlations of all core shells, but we find the most important correlation corrections for the levels we consider.

First we separate all single-electron orbitals of an atom into three categories: core, valence, and virtual states. We will construct the value of A from two parts: The first has been described and is given by Eq. (23), and the second can be represented in a similar form as

$$A_{\rm iso} = \sum_{\alpha,\beta} c_\alpha c_\beta \left\langle \Phi_\alpha \left| \sum_i r^{-3}[\mathbf{r}_i \times \boldsymbol{\alpha}_i]_0 \right| f_\beta \right\rangle . \quad (32)$$

Here f_β are determinant wave functions, defined by the DF procedure and Φ_α are determinant wave functions of virtual orbitals. It is now evident that the calculation of A in the frozen core approximation is based on the DF basis set only, while virtual orbitals are used for the calculation of $A_{\rm iso}$.

D. Theoretical results and comparison with experimental data

A numerical calculation of hfs constants was carried out for scandium ions in two different approximations: frozen core and polarization of the $3s$ and $3p$ core shells. The discrete spectrum of Sc II includes two-electron states with the ground configuration $3d4s$. The excited configurations are formed as a result of excitation of the $3d$ and $4s$ electrons. Our calculations include two groups of levels belonging to both even ($3d_{3/2}4s$, $3d_{5/2}4s$, $3d_{3/2}5s$, $3d_{5/2}5s$, $3d_{3/2}6s$, $3d_{5/2}6s$, $3d^2_{3/2}$, $3d^2_{5/2}$, $3d_{3/2}3d_{5/2}$, $4p^2_{3/2}$, $4p_{1/2}4p_{3/2}$) and odd ($3d_{3/2}4p_{1/2}$, $3d_{5/2}4p_{1/2}$, $3d_{3/2}4p_{3/2}$, $3d_{5/2}4p_{3/2}$) configurations in the jj coupling scheme.

The core shells were calculated in the presence of the $3d_{3/2}4s$ ground orbitals for the even configurations and

the $3d_{3/2}4p_{1/2}$ for the odd configurations. The theoretical values of A obtained in the frozen-core approximation are given in Table VI, column 1, and the values of B with this method are given together with experimental results in Table II. The experimental and the theoretical B values of the ground level have opposite signs, which may be caused by several reasons. The most important reason is probably that this level is the leading candidate to be perturbed by the Sternheimer shielding effect. We must also consider the large uncertainties in the experimental B value for the ground state, which was pointed out in Sec. II B. It can be seen in Table II that in general the agreement is good for the B values, particularly for the $3d4s$ and $3d^2$ configurations. However, some $3d4p$ levels show different signs for measured and for calculated B values. There is no obvious explanation for this discrepancy.

A comparison between our calculated A values and the values obtained with the same method in Ref. [5] is given in Table VI, columns 1 and 2. There is good agreement for most levels of the $3d4p$ configuration, which indicates a weak dependence of the numerical results on the specific features of the MCDF approach.

It is of special interest to compare experimental (Table II, column 3) and theoretical (Table VI, column 1) A values for the $3d^2$ configuration, because it is the first candidate to be affected by core polarization. We have very good agreement for the levels $^3F_2$, $^1D_2$, and $^1G_4$, while there are dramatic discrepancies for the levels $^3P_1$ and $^3P_2$. This discrepancy is, as expected, directly related to the core-polarization effect. The same situation is observed for the $3d4s$ configuration. Disagreement between A_{calc} and A_{meas} is about 42% for the ground state in the frozen-core approximation, but the sign is the same. The other values of A for the $3d4s$ configuration have better accuracies: 10.8%, 7.0%, 26.5% for the $^3D_2$, $^3D_3$, and $^1D_2$ levels, respectively.

There are different sources for the discrepancies between experimental and theoretical A values in $3d4s$ and $3d^2$ configurations. In particular the $4s$ electron in the ground state penetrates deeply into the atomic core, where it perturbs the core s electrons. We expect that the $3s$ orbital is dominant in this interaction because of the greater overlap between $3s$ and $4s$ electrons than, e.g., between $2s$ and $4s$ electrons. The explanation of the poor theoretical values for some of the levels in the $3d^2$ configuration requires the consideration of several factors. The amplitude of the $3d$ wave function at the nucleus is significantly smaller than for the $4s$ electron, so at first sight it seems that the interaction at the nucleus due to polarization effects should be weaker for the $3d$ electrons. On the other hand, the small amplitude of the $3d$ function at the nucleus should be very sensitive to various influences, such as polarization of the $3p^2_{1/2}$ and the $3p^4_{3/2}$ shells.

We have included the core-polarization effect for those levels in the $3d4s$ and $3d^2$ configurations that have poor agreement with experimental results. The computation procedure was organized in the following way. First we calculated a basis set of DF functions of Sc II for the considered configurations. Then we constructed the virtual orbitals as shown in Eq. (31) by exciting one of the core electrons to the virtual orbital. In the present work we take into account the polarization of three core shells: $3s^2$, $3p^2_{1/2}$, and $3p^4_{3/2}$.

The excitation of $3s^2$ into virtual states [Eq. (31)] was used to improve the value of A for the $3d4s\ ^3D_1$ level. Column 3 of Table VI gives the new values of A, which we obtained in the frame of the core-polarization approximation, using only the three first terms [$n=1,2,3$ in Eq. (31)] of the basis set. A comparison with experimental values now shows excellent agreement for $^3D_1$ and $^3D_2$, and some improvement for $^1D_2$. To obtain better theoretical values of A for the $3d^2$ configuration we excited both the $3s$ and the $3p$ core shells. This was first done for only the $3p_{3/2}$ shell, taking into account only one term with $n=1$ of Eq. (31), then we also opened the $3p_{1/2}$ shell ($n=1$) and in some cases we excited the $3s$ shell ($n=1$) as well. These data are shown in Table VI, column 3.

Our best theoretical A values, obtained with frozen-core or core polarization, are presented in Table II, column 4 together with the experimental values (column 3). The differences between experiment and theory are given in column 5. In our experiments only the $3d4s$ lev-

TABLE VI. MCDF values of the hyperfine coupling constant A for the configurations $3d4s$, $3d^2$, and $3d4p$ in Sc II. The core shells, which were polarized in our theoretical model, are shown within parentheses.

Level	A_{calc} (MHz)	A_{calc} [a] (MHz)	A_{calc} (MHz) Core polarization
$3d4s\ ^3D_1$	−279.7		−473.3
$3d4s\ ^3D_2$	453.4		518.8
$3d4s\ ^3D_3$	608.5		
$3d4s\ ^1D_2$	161.9		146.8
$3d^2\ ^3F_2$	277.6		
$3d^2\ ^3F_3$	179.2		143.5 ($3p_{3/2}+3s$)
			137.5 ($3p_{3/2}+3p_{1/2}$)
$3d^2\ ^3F_4$	138.6		85.6 ($3p_{3/2}$)
			63.3 ($3p_{3/2}+3p_{1/2}$)
			60.9 ($3p_{3/2}+3s$)
$3d^2\ ^1D_2$	146.0	146.6	
$3d^2\ ^3P_1$	10.3	−1.8	−63.6 ($3p_{3/2}+3s$)
$3d^2\ ^3P_2$	113.1	85.9	−0.03 ($3p_{3/2}$)
$3d^2\ ^1G_4$	154.6	143.2	
$3d4p\ ^1D_2^\circ$	202.5	202.4	
$3d4p\ ^3F_2^\circ$	425.3	309.2	
$3d4p\ ^3F_3^\circ$	193.7	193.8	
$3d4p\ ^3F_4^\circ$	115.6		
$3d4p\ ^3D_1^\circ$	267.7	278.3	
$3d4p\ ^3D_2^\circ$	149.0	165.5	
$3d4p\ ^3D_3^\circ$	128.3	134.4	
$3d4p\ ^3P_1^\circ$	148.0	167.1	
$3d4p\ ^3P_2$	87.2	96.6	
$3d4p\ ^1F_3^\circ$	184.9	178.2	

[a]Reference [5].

TABLE VII. Theoretical values of the hyperfine coupling constants for the $3d5s$ and $3d6s$ configurations in Sc II.

Level	Energy (cm^{-1})	A_{calc} (MHz)	B_{calc} (MHz)
$3d5s\ ^3D_1$	57 551.88	85.3	22.4
$3d5s\ ^3D_2$	57 614.40	293.4	−12.3
$3d5s\ ^3D_3$	57 743.92	−130.8	23.4
$3d5s\ ^1D_2$	58 252.09	151.2	−25.0
$3d6s\ ^3D_1$	77 195.19	337.1	11.0
$3d6s\ ^3D_2$	77 256.99	266.0	−13.8
$3d6s\ ^3D_3$	77 387.17	225.2	−35.6
$3d6s\ ^1D_2$	77 833.88	142.6	−25.3

els of the $3dns$ series were measured. An extension of hfs measurements to the next terms of this series should be very interesting, since theoretical values of A constants for the $3d5s$ levels show an irregular behavior (Table VII).

IV. CONCLUSION

We have measured the hfs of levels in the lower configurations in Sc II. A frequency-doubling system offered the opportunity to measure the hfs of the ground configuration. The experimental results were analyzed in terms of effective parameters. The semiempirical effective-operator method has the advantage of being a straightforward technique that provides information about the most important contributions to the hfs. It is not possible to extract very detailed knowledge about the fundamental interactions by examining the effective radial parameters. This is due to the difficulties in distinguishing between the different effects included in the parameters. We can, however, extract some qualitative information about the hyperfine interaction from the analysis.

The MCDF calculation in the frozen-core approximation gives, as a rule, realistic values of the A and B hfs constants for Sc II. The exception is represented by a few low-lying levels, for which A and B are comparable in magnitude but opposite in sign. In order to improve these data we made a core polarization calculation, using an alternative approach. In the frame of this approach we created a virtual basis set, with similar properties as Sturm's functions, i.e., orthogonalized and localized inside the core. By using only a few of these orbitals we reached significant improvement of A for the $3d4s$ levels and enhanced agreement for the $3d^2$ levels. It is possible that the hfs calculations may be improved with reasonably increased calculational efforts by increasing the number of terms of the virtual basis set Eq. (31).

ACKNOWLEDGMENTS

One of us (S.K.) gratefully acknowledges the hospitality of Uppsala University, Sweden, where joint work of this paper was initiated and performed. We thank Dr. I. I. Tupitzin for useful discussions as well as for help creating the computer program. Dr. S. Lunell is kindly acknowledged for reading the manuscript. This work has been supported by the Swedish Natural Science Research Council (NFR) and the Knut and Alice Wallenberg foundation.

*Fax: +46 - 18 18 35 24.
†Present address: Vrije Universiteit, Postbus 7161, 1007 MC Amsterdam, The Netherlands.

[1] N. Grevesse, J. Phys. (Paris) **4**, 181 (1991), and private communication.
[2] G. Olsson and A. Rosén, Phys. Rev. A **25**, 658 (1982).
[3] P. Villemoes, A. Wännström, A. Arnesen, R. Hallin, F. Heijkenskjöld, A. Kastberg, C. Nording, and O. Vogel, Z. Phys. D **18**, 235 (1991).
[4] A. Arnesen, R. Hallin, O. Staaf, L. Ward, B. Jelénkovic', M. Kisielinski, L. Lundin, and S. Mannervik, Astron. Astrophys. **106**, 327 (1982).
[5] L. Young, W. J. Childs, T. Dinneen, C. Kurtz, H. G. Berry, L. Engström, and K. T. Cheng, Phys. Rev. A **37**, 4213 (1988).
[6] N. B. Mansour, T. Dinneen, L. Young, and K. T. Cheng, Phys. Rev. A **39**, 5762 (1989).
[7] P. G. H. Sandars and J. Beck, Proc. R. Soc. London, Ser. A **289**, 97 (1965).
[8] G. H. Fuller, J. Phys. Chem. Ref. Data **5**, 835 (1976).
[9] D. M. Chipman, J. Chem. Phys. **78**, 3112 (1983).
[10] H. F. Schaefer, R. A. Klemm, and F. F. Harris, Phys. Rev. **176**, 49 (1968); **181**, 137 (1969).
[11] R. Glass and A. Hibbert, J. Phys. B **9**, 875 (1976); **11**, 2257 (1978).
[12] A. Hibbert, Rep. Prog. Phys. **38**, 1217 (1975).
[13] L. B. Jr. Knight, K. D. Johannessen, D. C. Cobranchi, E. A. Earl, D. Feller, and E. R. Davidson, J. Chem. Phys. **87**, 885 (1987).
[14] D. Feller and E. R. Davidson, J. Chem. Phys. **80**, 1006 (1984); Theor. Chim. Acta **68**, 57 (1989).
[15] D. Feller and E. R. Davidson, J. Chem. Phys. **90**, 1024 (1988).
[16] P. Kristiansen and L. Veseth, J. Chem. Phys. **84**, 6336 (1986).
[17] U. Kaldor and F. E. Harris, Phys. Rev. **183**, 1 (1969); Phys. Rev. A **1**, 1586 (1970); **2**, 1267 (1970).
[18] B. Engels, S. D. Peyerimhoff, and E. R. Davidson, Mol. Phys. **62**, 109 (1987).
[19] B. Engels and S. D. Peyerimhoff, J. Phys. B **21**, 3459 (1988).
[20] C. W. Jr. Bauschlicher, J. Chem. Phys. **92**, 518 (1990).
[21] S. Johansson and U. Litzén, Phys. Scr. **22**, (1980).
[22] J. Sugar and C. Corliss, J. Phys. Chem. Ref. Data **14**, 115 (1985).
[23] E. U. Condon and G. H. Shortley, The Theory of Atomic Spectra (Cambridge University Press, Cambridge, England, 1989).

[24] D. Taupin, *probabilities, data reduction and error analysis in the physical science* (Les Editions de Physique, France, 1988).
[25] W. J. Childs, Phys. Rev. A **2**, 316 (1970).
[26] H. Kopferman, *Nuclear Moments,* translated by E. E. Schneider (Academy, New York, 1958), pp. 445–449.
[27] S. A. Kotochigova and I. I. Tupitsyn, Opt. Spektrosk. **60**, 8 (1986) [Opt. Spectrosc. (USSR) **60**, 4 (1986)].
[28] E. Schrödinger, Ann. Phys. (Leipzig) **80**, 437 (1926).
[29] E. A. Hylleraas, Z. Phys. B **48**, 469 (1928).
[30] H. Shull and P. O. Löwdin, J. Chem. Phys. **23**, 1362 (1955); **30**, 617 (1959).
[31] S. Lunell, Phys. Rev. **173**, 85 (1968).
[32] A. I. Sherstyuk and P. F. Gruzdev, Opt. Spektrosk. **42**, 1198 (1977) [Opt. Spectrosc. (USSR) **42**, 690 (1977)].
[33] P. F. Gruzdev, G. S. Soloveva, and A. I. Sherstyuk, Opt. Spektrosk. **58**, 246 (1985) [Opt. Spectrosc. (USSR) **58**, 148 (1985)].